NAVAL POSTGRADUATE SCHOOL

MONTEREY, CALIFORNIA

THESIS

ONSHORE WIND STRESS AND BUOYANCY FLUX OBSERVED ON A DISSIPATIVE MEDITERRANEAN BEACH

by

Darin H. Keeter

December 2015

Thesis Advisor: Jamie MacMahan
Co-Advisor: Qing Wang

Approved for public release; distribution is unlimited

THIS PAGE INTENTIONALLY LEFT BLANK

REPORT DOCUMENTATION PAGE			Form Approved OMB No. 0704–0188
Public reporting burden for this collection of information is estimated to average 1 hour per response, including the time for reviewing instruction, searching existing data sources, gathering and maintaining the data needed, and completing and reviewing the collection of information. Send comments regarding this burden estimate or any other aspect of this collection of information, including suggestions for reducing this burden, to Washington headquarters Services, Directorate for Information Operations and Reports, 1215 Jefferson Davis Highway, Suite 1204, Arlington, VA 22202-4302, and to the Office of Management and Budget, Paperwork Reduction Project (0704-0188) Washington, DC 20503.			
1. AGENCY USE ONLY ***(Leave blank)***	**2. REPORT DATE** December 2015	**3. REPORT TYPE AND DATES COVERED** Master's thesis	
4. TITLE AND SUBTITLE ONSHORE WIND STRESS AND BUOYANCY FLUX OBSERVED ON A DISSIPATIVE MEDITERRANEAN BEACH			**5. FUNDING NUMBERS**
6. AUTHOR(S) Darin H. Keeter			
7. PERFORMING ORGANIZATION NAME(S) AND ADDRESS(ES) Naval Postgraduate School Monterey, CA 93943-5000			**8. PERFORMING ORGANIZATION REPORT NUMBER**
9. SPONSORING /MONITORING AGENCY NAME(S) AND ADDRESS(ES) N/A			**10. SPONSORING / MONITORING AGENCY REPORT NUMBER**
11. SUPPLEMENTARY NOTES The views expressed in this thesis are those of the author and do not reflect the official policy or position of the Department of Defense or the U.S. Government. IRB Protocol number ____N/A____.			
12a. DISTRIBUTION / AVAILABILITY STATEMENT Approved for public release; distribution is unlimited			**12b. DISTRIBUTION CODE**

13. ABSTRACT (maximum 200 words)

A five-month study was performed on an energetic, dissipative beach on a climatologically Mediterranean coastline to explore the wind stress and buoyancy flux. An eddy covariance system was deployed in the intertidal zone resulting in 1088 hours of quality-controlled flux observations at elevations of 1, 3, and 6m on a sandy beach in Monterey, CA. The wind stress angle relative to the mean wind direction varied as much as 31^{o}, representing one standard deviation, with a range of $\pm 151^{o}$. The variations were dependent on the wind angle relative to the swell direction and shoreline, which directed the stress vector to the left for winds approaching from $0^{o}>\theta>-45^{o}$ and to the right for winds approaching from $-45^{o}>\theta>-80^{o}$, where 0^{o} is onshore. The stress angle was independent of stability, stress, and wind speed. Air-ocean temperature differences produced unstable conditions 88% of the time in contrast to the near neutral conditions that dominate the open ocean. Based on flux footprints, the surf zone was found to be a source of positive buoyancy and heat flux contributing to the unstable conditions. Minimum buoyancy fluxes were observed with the flux footprints that were farther offshore centered outside the surf zone, resulting in stable conditions.

14. SUBJECT TERMS wind stress, stress angle, buoyancy flux, eddy covariance, nearshore, surf zone			**15. NUMBER OF PAGES** 61
			16. PRICE CODE
17. SECURITY CLASSIFICATION OF REPORT Unclassified	**18. SECURITY CLASSIFICATION OF THIS PAGE** Unclassified	**19. SECURITY CLASSIFICATION OF ABSTRACT** Unclassified	**20. LIMITATION OF ABSTRACT** UU

THIS PAGE INTENTIONALLY LEFT BLANK

Approved for public release; distribution is unlimited

ONSHORE WIND STRESS AND BUOYANCY FLUX OBSERVED ON A DISSIPATIVE MEDITERRANEAN BEACH

Darin H. Keeter
Lieutenant Commander, United States Navy
B.A., Thomas Edison State, 2009

Submitted in partial fulfillment of the
requirements for the degree of

MASTER OF SCIENCE IN METEOROLOGY AND PHYSICAL OCEANOGRAPHY

from the

NAVAL POSTGRADUATE SCHOOL
December 2015

Approved by: Jamie MacMahan
Thesis Advisor

Qing Wang
Co-Advisor

Timour Radko
Chair, Department of Oceanography (Acting)

THIS PAGE INTENTIONALLY LEFT BLANK

ABSTRACT

A five-month study was performed on an energetic, dissipative beach on a climatologically Mediterranean coastline to explore the wind stress and buoyancy flux. An eddy covariance system was deployed in the intertidal zone resulting in 1088 hours of quality-controlled flux observations at elevations of 1, 3, and 6m on a sandy beach in Monterey, CA. The wind stress angle relative to the mean wind direction varied as much as 31^o, representing one standard deviation, with a range of $\pm 151^o$. The variations were dependent on the wind angle relative to the swell direction and shoreline, which directed the stress vector to the left for winds approaching from $0^o > \theta > -45^o$ and to the right for winds approaching from $-45^o > \theta > -80^o$, where 0^o is onshore. The stress angle was independent of stability, stress, and wind speed. Air-ocean temperature differences produced unstable conditions 88% of the time in contrast to the near neutral conditions that dominate the open ocean. Based on flux footprints, the surf zone was found to be a source of positive buoyancy and heat flux contributing to the unstable conditions. Minimum buoyancy fluxes were observed with the flux footprints that were farther offshore centered outside the surf zone, resulting in stable conditions.

THIS PAGE INTENTIONALLY LEFT BLANK

TABLE OF CONTENTS

THIS PAGE INTENTIONALLY LEFT BLANK

LIST OF FIGURES

THIS PAGE INTENTIONALLY LEFT BLANK

LIST OF TABLES

THIS PAGE INTENTIONALLY LEFT BLANK

ACKNOWLEDGMENTS

To my advisor, Dr. Jamie MacMahan, thank you for encouraging me and providing me the autonomy to pursue original research. To my co-advisor, Dr. Qing Wang, thank you for the latitude in my pursuits and patience when it came to the math. I'd like to thank Dr. Reginald Beach, ONR Coastal Dynamics program officer, for taking an interest in and agreeing to fund my research.

To my classmates, thank you all for your willingness to lend a hand whenever I asked and provide some intellectual calibration whenever I needed it.

There are a few people I'd be remiss if I did not thank personally. On the oceanography side, to Mr. Keith Wyckoff for his enthusiasm and for helping out with equipment builds, deployments and most importantly, equipment recovery; Mr. Mike Cook for his invaluable assistance with MATLAB and willingness to help out with the fieldwork. To Professor Tim Stanton, thanks for helping with the electrical issues and not allowing me to electrocute myself. On the meteorology side, thanks to Mr. Dick Lind, whose guidance on equipment capabilities, help building gear for the initial class project and assistance moving data around. I know it was the "most" you could do. Mr. Ryan Yamaguchi, your assistance and guidance when it came to programming instruments and data loggers was invaluable.

THIS PAGE INTENTIONALLY LEFT BLANK

I. INTRODUCTION

Wind stress, τ, or the transfer of momentum between the atmosphere and the underlying ocean has long been recognized as a critical parameter in ocean and climate modeling and in the processing of remote sensing satellite data. The surface wind stress can be represented through the friction velocity u_* (Monin and Obukhov 1954), defined as

$$\tau = -\rho_a u_*^{\,2} \ , \tag{1}$$

where ρ_a is atmospheric density. This wind stress is therefore dependent on the roughness properties of the underlying surface. The ocean, however, is a fluid that changes with the application of stress. Here the “roughness” of the water and the atmospheric friction velocity change in as little as a few minutes. These changes are often described using the well-known equation from Charnock (1955)

$$z_0 = m\frac{u_*^{\,2}}{g} \ , \tag{2}$$

where z_0 is the surface roughness length of the ocean, g is acceleration due to gravity, and m is the non-dimensional coefficient known as the Charnock Coefficient. Due to the difficulty in measuring τ directly, and the need for efficient calculation methods for modeling purposes, τ is often calculated using easily measured or forecast parameters through the bulk formula,

$$\tau = -\rho_a C_D \overline{U}^2 \ , \tag{3}$$

where C_D is the drag coefficient and $\overline{U}$ is the mean horizontal wind speed at a given level within the atmospheric surface layer. According to Monin-Obukhov

similarity theory (MOST) (Monin and Obukhov 1954) the stress in the surface layer is near constant. None of the terms in equation (3) depend on direction, which suggests that τ must be aligned with $\overline{U}$.

Numerous studies were performed over the past four and half decades with the aim of improving the bulk formula parameterizations (Businger et al. 1970; Large and Pond 1980; Geernaert 1990; Rieder et al. 1994; Edson et al. 2013). However, many of these studies assumed that all stress is stream wise and neglected any cross-stream stress, in line with MOST. A few recent studies however, have found that the stress vector is often not aligned with the stream wise wind vector (Potter 2015; Rieder et al. 1994; Geernaert et al. 1988; Zemba and Friehe 1987). The difference between these two vectors is referred to as the stress angle, α.

These deviations from MOST can be significant (Zhang et al. 1980) and are attributed to various processes such as surface sensible heat flux (Geernaert et al. 1988), coastal jets (Zemba and Friehe, 1987), and sea/swell direction (Grachev et al. 2003; Geernaert et al. 1993). Rieder and Smith (1998) found that wind stress vector was directed away from the mean wind direction and toward the wave direction for both swell and wind sea waves. Riechl et al. (2014) found that swell moving at an oblique angle to the wind tends to increase the misalignment between the wind vector and the stress vector in tropical storms.

These studies improved our understanding of wind stress and the stress angle in the open ocean, and led to improvements in bulk algorithms (Fairall et al. 2003) and the use of satellite based scatterometer data, which were shown to be sensitive to the stress angle (Liu et al. 2007; Rufenach et al. 1998). Little work, however, was done to quantify wind stress or explain the presence of the stress angle in the nearshore environment. Two recent exceptions, Shabani et al. (2014) and Ortiz-Suslow et al. (2015), highlighted how different this environment is from the open ocean. Ortiz-Suslow et al. (2015) utilized a mobile platform to perform direct flux measurements in the vicinity of the New River Inlet (NRI) on

the North Carolina Coast exploring the relationship between wind stress and currents using a mobile platform that enabled measurements to be taken from within the inlet to approximately 4000m offshore. The NRI data set measured stress angles that were up to 60° off from the mean wind. Shabani et al. (2014) performed direct measurements of wind stress over the surf zone from a fixed tower on the beach where a strong relationship between the wind stress and cross-shore wind angle existed with significantly less stress associated with along shore winds. Both studies found values of C_D that were about twice that found in the open ocean.

This thesis presents the results of a five-month study of the nearshore environment on a Mediterranean beach (Johnson 1977) extending from the intertidal zone through the surf zone to the adjacent inner shelf. During this study, the eddy covariance method is used to obtain direct measurements of the wind stress and buoyancy flux using a portable tripod that was deployed near the high tide water line. The results provide a detailed picture of the nature of wind stress and the stress angle and stability in the nearshore environment that will hopefully lead to improvements in nearshore modeling.

THIS PAGE INTENTIONALLY LEFT BLANK

II. THEORETICAL BACKGROUND

A. WIND STRESS

Unlike bulk methods, an eddy covariance system provides direct measurements of fluxes. In this application τ is defined by the Reynolds shear stress

$$\tau = -\rho_a(\overline{u'w'} + \overline{v'w'}) \ , \tag{4}$$

where ρ_a is atmospheric density and u', v', w' are the turbulent fluctuations of the wind velocity in the stream wise, cross-stream and vertical axes, respectively. The overbar represents that the data are averaged over some appropriate period. In the direct method shear velocity is defined as

$$u_* = \left(\overline{u'w'}^2 + \overline{v'w'}^2\right)^{\frac{1}{4}} \ , \tag{5}$$

By MOST, the mean wind gradient is related to the friction velocity by

$$\frac{\partial \overline{U}}{\partial z} = \frac{u_*}{\kappa z}\phi_m\left(\frac{z}{L}\right) \ , \tag{6}$$

where $\kappa = 0.4$ is the von Karman constant, z is the height above the surface, and ϕ_m is the dimensionless velocity gradient function that depends on z and the Monin-Obukhov length L, which is defined as

$$L = -\frac{u_*^{\,3}\overline{T_v}}{g\kappa\overline{T_v'w'}} \ , \tag{7}$$

where $\overline{T_v}$ represents the mean virtual temperature in Kelvin. The sonic temperature T_s is a suitable approximation for T_v (Kaimal and Gaynor 1991) and will be used for calculations in this study. Integrating equation (6) from the roughness height z_0 to the measurement height z yields

$$\overline{U} = \frac{u_*}{\kappa}\left[\ln\frac{z}{z_0} - \psi_m\left(\frac{z}{L}\right)\right]. \tag{8}$$

The first term in the square bracket in equation (8) is the classic log wind profile for neutral stability. The stability function ψ_m is related to the MOST velocity gradient function ϕ_m in equation (6), and defines how deviations from neutral stability modify the logarithmic wind profile. The velocity gradient ϕ_m can be expressed as in equations (9) and (10) based on Businger et al. (1971)

$$\phi_m\left(\frac{z}{L}\right) = \left(1 - \alpha_b\frac{z}{L}\right)^{-\frac{1}{4}} \text{ for } \frac{z}{L} < 0 \text{ (unstable)} \tag{9}$$

$$\phi_m\left(\frac{z}{L}\right) = 1 + \beta_b\frac{z}{L} \text{ for } \frac{z}{L} > 0 \text{ (stable).} \tag{10}$$

For this study the values of the coefficients are $\alpha_b = 20$ and $\beta_b = 5$ as in Shabani et al. (2014) and Yelland and Taylor (1996). Following Paulson (1970), ψ_m can be expressed in unstable conditions $(z/L < 0)$ as

$$\psi_m\left(\frac{z}{L}\right) = 2\ln\left(\frac{1+\phi_m^{-1}}{2}\right) + \ln\left(\frac{1+\phi_m^{-2}}{2}\right) 1 - \phi_m \\ -2\tan^{-1}\left(\phi_m^{-1}\right) + \frac{\pi}{2}. \tag{11}$$

While for unstable conditions Lo and McBean (1978) have derived that ψ_m can be evaluated by

$$\psi_m\left(\frac{z}{L}\right) = 1 - \phi_m = -5\frac{z}{L} \ . \tag{12}$$

Stress is often parameterized in terms of the drag coefficient in flux calculations from observations as well as in numerical modeling. Rearranging equation (3), one can explicitly define drag as

$$C_{Dz} = \frac{\tau}{\rho_a \overline{U_z}^2} = \left(\frac{u_*}{\overline{U_z}}\right)^2 \ , \tag{13}$$

where the subscript z denotes the height of the measurement or calculation.

It is important to be able to compare drag coefficients from various studies and model output. However, the dependency of C_D on the thermal stability regime makes the comparison problematic. In order to make these comparisons, the drag coefficients are normally converted to neutral stability conditions following Geernaert et al. (1987) according to

$$C_{DNz} = \left[C_{Dz}^{-\frac{1}{2}} + \frac{\psi_m\left(\frac{z}{L}\right)}{\kappa} \right]^{-2} \ . \tag{14}$$

Since the measurements are not necessary made at the same height above the surface it is also common practice to report C_{DN} in reference to a

common altitude, normally 10m using wind input from 10 m. The log wind profile is used to relate the wind speeds and drag coefficients between the measurement and reference level according to

$$\frac{C_{DNz_2}}{C_{DNz_1}} = \left(\frac{\overline{U_{Nz_1}}}{\overline{U_{Nz_2}}} \right)^2 = \left(\frac{\ln \frac{z_1}{z_0}}{\ln \frac{z_2}{z_0}} \right)^2 , \quad (15)$$

where z_1 represents the measurement height and z_2 the new reference height, in this case 10 m. Equation (15) is only applicable to neutral thermal stability.

Fluxes obtained using the eddy covariance method also allow for the obtaining the stress angle α, the angle between the mean wind vector and the wind stress vector as

$$\alpha = (\overline{v'w'} / \overline{u'w'}) , \quad (16)$$

where $\alpha = 0$ indicates that the stress and wind vectors are aligned while positive (negative) values indicate that the stress vector is directed to the left (right) of the wind vector by α degrees.

Another parameter often associated with eddy covariance measurements is the buoyancy flux or sensible heat flux H_s (Geernaert et al. 1987)

$$H_s = \rho_a c_p \overline{w'T_s'} , \quad (17)$$

where c_p is the specific heat of air at constant pressure. This flux represents the flux between the surface and the atmosphere. Positive (negative) indicates the surface is a source (sink) for heat energy.

III. METHODS

A. DEL MONTE BEACH

The study site was located on Del Monte beach, in Monterey, CA. This beach is a northwest facing, sandy beach in the topographically sheltered southern portion of the Monterey Bay, Figure 1. The slope of the beach ranges from 1:14 to 1:40 with predominantly plunging and spilling type breakers (Thornton et al. 1976). Tides are mixed with a diurnal range of approximately 2m between the highest and lowest tide. The topographic features of the surrounding area limit the fetch for significant local seas development to only regimes with northerly winds. Pacific Ocean swells undergo wave refraction due to interactions with the sandy shelf, which results in swells that are consistently normal to the beach (MacMahan et al. 2005). The climate is Mediterranean in nature, characterized by the cool California current that moderates the temperatures maritime air and the warm dry inland regions, (Johnson 1977). Winds are dominated by a daily sea breeze that develop due to strong thermal gradients between the relatively cool maritime air and the inland valley due to diurnal heating (Hendrickson and MacMahan 2009).

Figure 1. Field Study Site

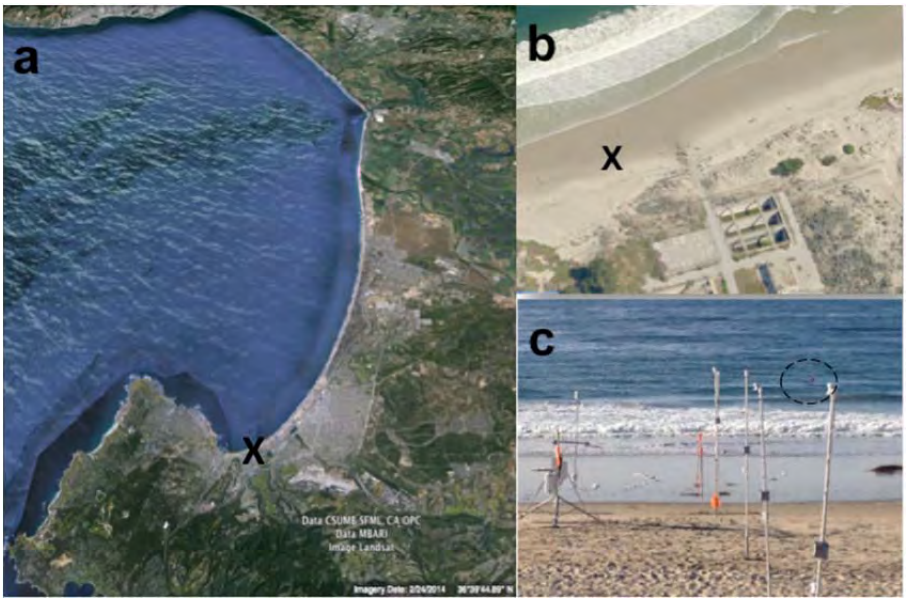

Google Earth image of Monterey Bay (a) and Bing Birdseye view of Del Monte Beach (b) both with the location of the Surf Flux Tripod deployments marked by an "x." Cross-shore view of study site (c) from March 19, 2015. Pictured are the SFT (left), fixed sensor stations (right) and buoy marking the location of the offshore temperature and pressure array.

1. Surf Flux Tripod

Eddy covariance measurements were obtained during 4 separate collection periods from March 16, 2015, to July 16, 2015, using a Surf Flux Tripod (SFT) Figure 2, resulting in the collection of 1088 hours of quality controlled flux data. Instrumentation included an R. M. Young Model 81000 3D Ultrasonic Anemometer, mounted at a height of 1m, two Campbell Scientific temperature and humidity probes, located at 1m and 3m, a downward looking infrared radiometer to measure the skin temperature of the water/sand directly in front of the SFT, and a Kipp and Zone CNR4 net radiometer to measure total solar and terrestrial radiation. On April 11, 2015, a second sonic anemometer was added at a height of 3m. All sensors were wired to a Campbell Scientific CR 3000 data logger for initial processing, and data were stored on a 2Gb compact flash data card as detailed in Table 1. Power for the SFT was provided by a 12V lead acid battery that was housed in a separate waterproof enclosure.

Table 1. Surf Flux Tripod Sensor Suite

Sensor	Height	Sample Rate
RMY81000 Sonic Anemometer (2)	1/3m (3/6 m)*	20 Hz
Temperature/humidity (2)	1/3m (3/6 m)*	1 Hz
Down looking radiometer	1.3 m	1 Hz
CNR4 Net Radiometer	1.6 m	1 Hz

*4th deployment only.

As mentioned the system was deployed over four separate collection periods. The moves between deployments 1–2 and 2–3 were necessitated due to beach erosion. The fourth deployment was to enable the SFT to be reconfigured with the sonic anemometers and temperature/humidity sensors at 3m and 6m. During the study period, the system was inspected daily and was cleaned to remove any salt or dirt from the instruments and kelp from around the tripod assembly as required. The battery was replaced every 4–5 days at which time the data was collected for processing. Specific deployment times locations and the reference beach elevation data can be seen in Table 2.

Table 2. Deployment Locations/Times

Deployment	Lat	Lon	Start*	Stop*	SFC re:MSL
1	36.6034	-121.8729	75.9418	106.5186	2.84m
2	36.6037	-121.8732	106.5781	125.8262	2.86m
3	36.6032	-121.8728	127.0052	149.8717	2.87m
4	36.6034	-121.8730	158.9019	197.0848	2.91m

*Start and stop times are in Julian/Decimal day UTC

Figure 2. Surf Flux Tripod

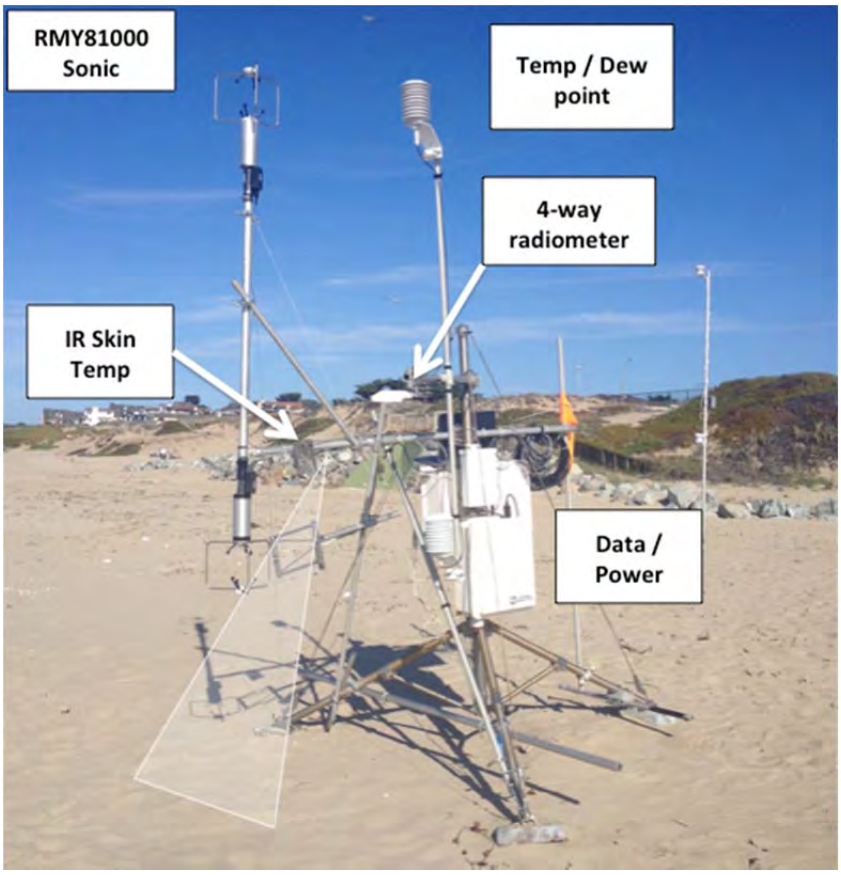

SFT deployed at Del Monte Beach on April 11, 2015.

2. Ocean Temperature and Waves

In order to characterize the ocean environment a temperature array was deployed approximately 70m offshore in 5m water depth. This array consisted of six Onset Tidbit temperature loggers attached to a weighted line with a surface float. Sensors were placed on the weight and at 1m intervals to the surface with the top sensor housed in a protective solar shield to prevent direct heating from the sun. Temperature sensors were initially deployed at a sampling rate of 60s but were reconfigured for a 5min sampling rate after the first retrieval. RBR pressure sensors (Solo and DR1050) were attached to the bottom weight in order to capture wave statistics. Pressure sensors sampled continuously at 1 Hz. The temperature sensors were downloaded periodically in the field using a

waterproof data shuttle, and pressure sensors were swapped-out during this time.

3. Beach Topography

A total of 10 walking surveys were conducted of the beach along an approximately 100m tract from the dry upper beach seaward out into the surf zone, using a high resolution Ashtech GPS system, which has a horizontal accuracy of O(1 cm). The surveys were conducted at the start and end of the study with additional surveys made after significant changes in beach morphology due to storm activity. The National Geodetic Survey (NGS) GEOID99 model was used to convert the vertical heights to NAVD88 vertical datum. Data were then transformed into a local coordinate system [X, Z] where X is directed cross-shore and increases seaward and Z is elevation referenced to local Mean Sea Level (MSL) using offsets obtained from the Monterey (MYXC1) tidal station (National Oceanic and Atmospheric Administration [NOAA] 2011). Using linear interpolation of the survey data, the beach elevation was then calculated for the entire study period and a common profile length.

B. DATA

1. Eddy Covariance

Following the methods outlined in Aubinet et al. (2012), the 20 Hz flux data from the sonic anemometers underwent quality control checks to remove data spikes caused by either instrumentation or natural events. The data converted to a shore normal reference frame before being rotated into the mean wind direction and a tilt correction was then applied using the planar fit method (Paw U et al. 2000; Wilczak et al. 2001) to ensure that the mean vertical velocity was equal to zero. Failure to perform the tilt correction can result in biasing of the vertical velocity due to upslope enhancement. Once the tilt correction was performed, then data were averaged in order to capture the needed statistics for use in eddy covariance calculations while still keeping the data averaging small enough to represent stationarity in the observations. A 15-minute averaging

period was selected for this effort, which is in line with the normal range of 10 to 30 minutes that have been used in other studies (Aubinet et al. 2012). Flux calculations were then made using the averaged and corrected data. Finally, post processing filters were applied for wind direction $\left(\pm 50^{\circ}\right)$ to ensure there was no contamination of the data due to turbulence induced by the tripod and by wind speed to remove winds less than 3 m/s for which flux measurements are not valid due to the lack of turbulent eddies. Additionally, records where the wind speed between the upper and lower anemometers was inconsistent indicating potential contamination of data due to stream blockage was eliminated.

2. Surface Meteorological

1Hz temperature and humidity data, skin temperature, and net-radiation sensor data from the SFT were quality-controlled to remove erroneous spikes. These data were also averaged over the same 15min periods as the flux data. Atmospheric pressure data was taken from the fixed meteorological station located at the Naval Postgraduate School's beach laboratory approximately 70m to the southeast of the study site. Data were reduced to MSL based on Babinet's formula (Smithsonian 1897) and reduced data were used to calculate atmospheric density.

3. Water Level

For this study we used the verified NOAA water level data from the Monterey, CA tidal station located 1500m west of the study site. The verified water level data was output in 6min time steps, and were then interpolated to the experiment time for use in calculating the cross-shore and stream wise distance between the SFT and the water's edge. Significant sand erosion and deposition caused vertical changes in the sand elevation of $\pm 1m$, Figure 3 (dashed red lines). This resulted in the migration of the mean higher high water (MHHW) mark on the beach by 20m in the cross-shore direction over the course of the study, Figure 3 (dotted blue line).

Figure 3. Beach Profile

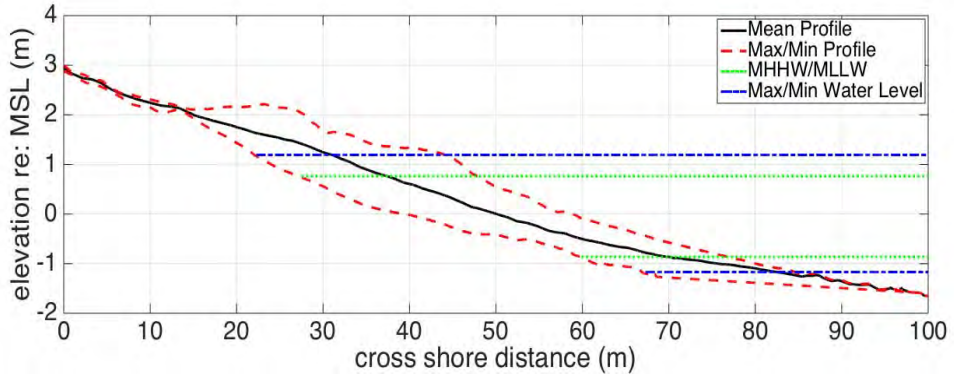

The mean beach profile for March through July 2015 is shown by the solid black line. Mean high high water and mean low low water levels are indicated by the dashed green line. The maximum and minimum observed water levels are indicated by the dashed blue line. All elevations are in meters and are referenced to local mean sea level.

C. ORIENTATION

The spatial and directional attributes of winds, waves, stresses etc., will be described using a local coordinate system in reference to the SFT and the shoreline. For ease of analysis and description, the angle $\theta = 0$ is defined as shore normal from the beach to the ocean with negative values to the left and positive values to the right. Wind direction is given in the meteorological convention with winds coming from a given angle. Vectors indicate the direction of travel (i.e., a wind direction of -90 would indicate wind traveling along shore from left to right, parallel with the shoreline). Note that due to wave refraction, swells are normally incident to the beach and approach the shoreline on a heading of 180. This reference frame represents wind normal to the shoreline as well as the incoming waves.

THIS PAGE INTENTIONALLY LEFT BLANK

IV. RESULTS

A. FLUX FOOTPRINT

For any eddy covariance measurements, there exists an upwind area that contributes to the properties of the quantities being measured. This area is often referred to as the flux footprint. In a completely homogeneous environment, such as a vast expanse of ocean or flat unchanging landscape, this is not a large issue. In a dynamic environment, where there are significant differences in the surface properties near the measurement site, there is a greater need to understand what source(s) may be contributing to the measured flux. Many researchers have attempted to quantify and provide solutions from computing the flux footprint from complex dispersion models to simple analytic solutions (Gash 1986; Schuepp et al. 1990; Schmid 1993). The goal for the purposes of this study is to be able to determine when the measured flux is primarily from over the water or the sandy shoreline given the relatively low measurement heights used in this study. The simple analytical solution proposed by Schuepp et al. (1990) that was implemented by Ortiz-Suslow et al. (2015) was chosen. This method allows for the calculation of the area of the footprint that the measurement is most sensitive according to

$$x_{\max} = \frac{U}{u_*}\frac{z}{2\kappa}\ , \tag{18}$$

where $x_{\max}$ is the distance in the stream wise direction from the sensor into the wind that has the largest contribution to the flux footprint. Knowing $x_{\max}$ and the cross-shore distance to the water x_w in the direction of the mean wind, a footprint ratio determines if the footprint is “wet” or “dry” according to

$$\frac{x_{\max}}{x_w} < 1 = Dry \tag{19}$$

$$\frac{x_{\max}}{x_w} \geq 1 = Wet \ , \tag{20}$$

with dry indicating that the max contribution comes from over the sandy beach/swash zone and wet indicating that the max contribution is from over the water. The majority of the footprints for the 3m and 6m heights are over the water, 74% and 80% respectively, Figures 4a, 4b, and 4c. However, only 10% of the 1m observations are over the water, owing the low elevation, Figures 4a and 4b.

Figure 4. Flux Footprint Ratio

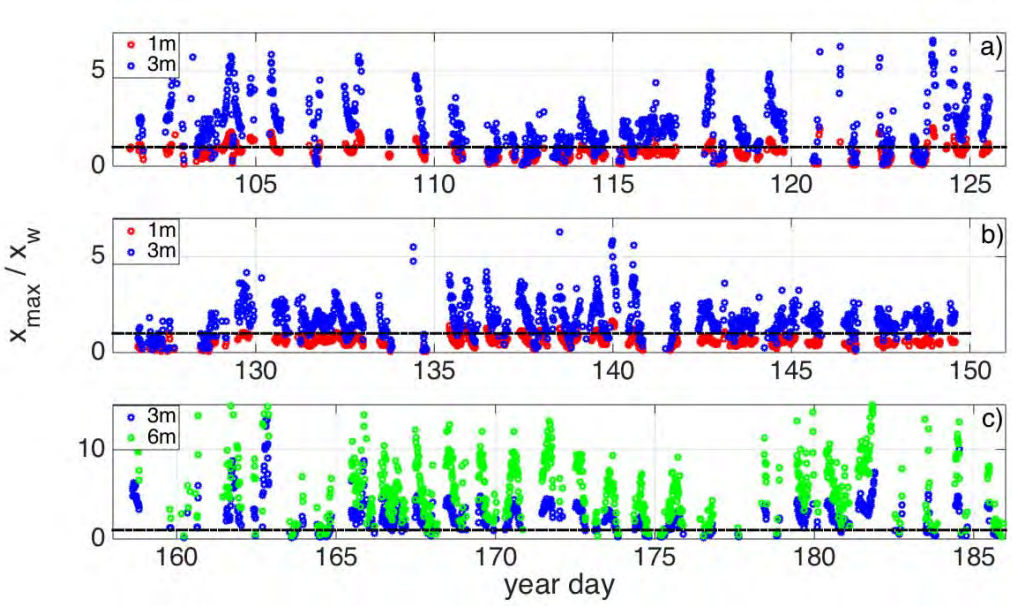

Time series of the ratio of $x_{\max}$ and x_w for the upper and lower anemometer pairs for (a) deployments 1 and 2 (b) deployment 3 and (c) deployment 4. The dashed black line on the y-axis indicates a ratio of 1 meaning all observations above that line are "wet" while all observations below that line are "dry." Each circle represents 15min of data from 1m (red circles), 3m (blue circles) or 6m (green circles).

B. STABILITY

The non-dimensional stability parameter z/L, from equation (7), represents the relationship between thermal and mechanical turbulent mixing in the surface layer. z/L is normally related to the flux of momentum, temperature and other scalar parameters through the use of the MOST stability functions. Under absolute neutral stability conditions, $z/L = 0$, development of turbulent fluxes are entirely dependent on mechanical shear induced by the flow of the wind over the surface. It is under these conditions that the well know log wind profile relating the mean wind speed, $\overline{U}$, and surface roughness, z_0, to measurement height is obtained. However, the atmosphere is very rarely in a state of absolute neutral stability. During stable conditions, $z/L > 0$, atmospheric stratification works to suppress turbulent fluxes from mixing upward while under unstable conditions when $z/L < 0$ thermal instability and convection work to enhance turbulent mixing.

Studies have generally classified atmospheric stability into three basic categories: unstable, near neutral, and stable. Near neutral is often defined as $-0.1 < z/L < 0.05$ (Smith 1980; Smith et al. 1991; Shabani et al. 2014). Near neutral conditions are expected over most of the ocean (Barale et al. 2010). However, data from this study suggest something quite different for the nearshore environment. The distribution of z/L measured from 3m and 1m during the first 3 deployment periods (Figure 5a) and from 6m and 3m during the fourth period (Figure 5b) show that a relatively small amount of the data are considered near neutral. In fact, these data are very similar to conditions measured over the flat wheat fields during the Kansas experiment of Kaimal et al. (1972), which had ranges of $-2.1 < z/L < 3.3$.

Figure 5. Stability $\left(\frac{z}{L}\right)$ Frequency of Occurrence

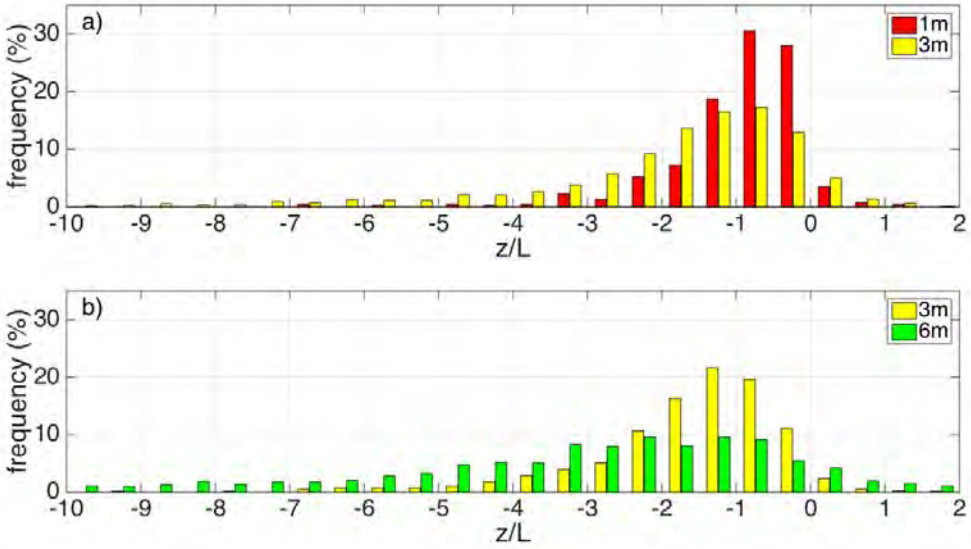

Stability distribution (a) for deployments 1–3 and (b) for deployment 4. The y-axis is frequency of occurrence and data are binned in intervals of 0.5. The data has been filtered to include only onshore winds where the foot print, defined by equation (18), is over the water. The data has also been filtered for $-10 < z/L < 2$ which fit more than 80% of the data from each anemometer height/deployment. Total u_* as defined in equation (5) was used for these calculations.

For each pair of anemometers, the upper elevation is more unstable than the lower elevation (Figure 5), consistent with Shabani et al. (2014). The 3m data, however, are fairly consistent across the entire study period with only slightly more instability during deployment four (Figure 5b, yellow bars). This is likely due to deployment four being conducted during the transition between spring and summer. This time period experienced warmer water temperatures associated with increased down welling short wave radiation due to longer days. Compared with Shabani et al. (2014), the stability observations here in Monterey, CA, result in more unstable scenarios that Shabani et al. 2014 found in Australia. As will be discussed later, this is believed to be associated with the air–ocean temperature differences, resulting in discrepancies between these two studies.

The majority of the conditions are found to be unstable range requiring further categorization, which if often ignored in other studies. A modified version of the three-layer classification system proposed by Kader and Yaglom (1990) is applied to further describe the various unstable regimes. The first category, the dynamic sublayer, $-0.04 \le z/L \le 0$, comprises the regime where thermal stability and buoyancy effects are relatively small and turbulent production is almost entirely driven by mechanical forcing. The next category, called the dynamic convective sublayer, $-1.20 \le z/L \le -0.12$, describes conditions where thermal instabilities become significant but do not yet dominate mechanical forcing. The final category is the free convective sublayer $-2.00 \le z/L \le -1.20$, which is characterized by a regime that is almost entirely dominated by thermal instability. This classification scheme implies that there are transitional layers exist between the three explicitly defined sublayers (Bernardes and Dias 2010). There also exists stable sublayer where atmospheric stratification suppresses the production of mechanical turbulence.

The distribution of z/L binned by the Kader and Yaglom classification can be seen in Figure 6. For the first set of data from deployments 1–3, 89% of the 3m and 92% of the 1m measurements fell into the convective sublayers (Figure 6a). For deployment 4, 88% of the 6m and 95% of the 3m data are described by convective sublayer categories (Figure 6b). These measurements indicate that the nearshore environment is much more unstable than the open ocean.

Figure 6. Kader and Yaglom Stability Classification

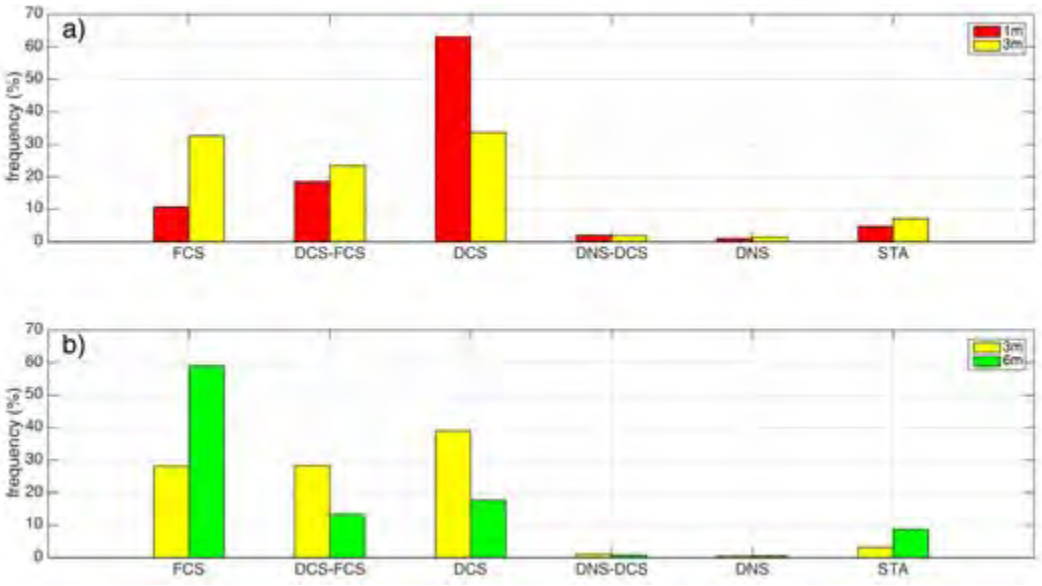

Kader and Yaglom stability classification (a) for deployments 1–3 and (b) for deployment 4. The y-axis is frequency of occurrence and data are binned in according to criteria listed in Table 2. The data has been filtered to include only onshore winds where the footprint, defined by equation (18), is over the water. The data has also been filtered for $-10 < z/L < 2$ which fit more than 80% of the data from each anemometer height/deployment. Total u_* as defined in equation (5) was used for these calculations and abbreviations are defined in Table 2.

C. BUOYANCY

Buoyancy flux, H_s, is closely related to stability through the temperature covariance term $\overline{T'w'}$ found in both equations (7) and (17). The sign of H_s indicates the direction of heat energy transfer between the atmosphere and the underlying surface. Positive flux associated with heat energy moving up into the atmosphere and negative flux indicates that heat energy moving down into the water. Air-water temperature differences, $\Delta T = T_a - T_w$, provides an estimate of the surface layer stability and buoyancy flux (Kara et al. 2005). A positive ΔT, or warm air over colder water is associated with increased stability and negative buoyancy flux for all deployments, Figure 7. Conversely, a negative ΔT, or cold air over warmer water is associated with greater thermal instability and positive buoyancy flux. For all deployments, buoyancy flux is seen to increase as

negative ΔT increases. For the 1m sensor height from deployments 1–3, Figure 7b, the range of values is much smaller that the corresponding 3m sensor, Figure 7a. This is due to the smaller footprint area, which is a function of height. A similar pattern is observed with the 3m sensor from deployment number 4, Figure 7d, and the 6m sensor, Figure 7c, for the same reason. For all deployments, the maximum buoyancy flux is not always associated with the maximum temperature difference indicating the other factors are also important in the determination of buoyancy flux.

Figure 7. Buoyancy Flux (z/L)

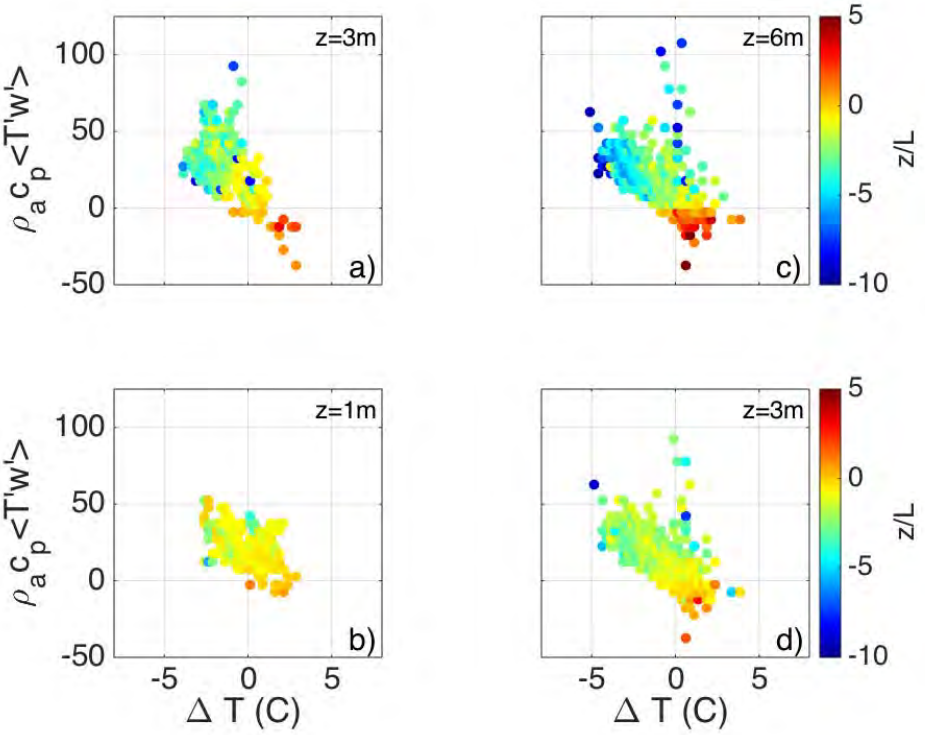

Buoyancy flux for deployments 1–3 (a) and (b) for and deployment 4 (c) and (d). The y-axis is buoyancy flux calculated according to equation (17). The x-axis is the temperature difference between the measurement height and the ocean surface temperature measured from the off shore array ($T_a - T_w$). Negative values indicate the ocean is warmer than the atmosphere and positive indicates that ocean temperatures are colder than the atmosphere. Data are shaded according to the stability parameter z/L. The data has been filtered to include only onshore winds where the footprint, defined by equation (18), is over the water.

Since the temperature covariance is an integral term in both H_s and z/L, it is relatively self-correlating, and requires an evaluation of other independent parameters. For the 6m height during the fourth deployment, a comparison of the heat flux versus hours of the day, net radiation, and relative humidity show that the highest consistent magnitude of buoyancy flux, approximately $45 Wm^{-2}$, is associated with the daytime maximum net radiation, Figures 8a and 8c. The ocean continues to be a source of positive H_s well after sunset, with a nighttime maximum of approximately $30 Wm^{-2}$, Figure 8a. The nighttime buoyancy flux is also associated with the maximum relative humidity levels, Figure 8b. These same patterns were also observed at1m and 3m.

Buoyancy flux is also a function of the cross-shore distance, $x_{\max}$. Minimum buoyancy flux values are associated maximum cross-shore extent of the flux footprint, $x_{\max}$, Figure 8d. As the footprint moves closer to shore, buoyancy flux values increase with the highest values associated with the minimum $x_{\max}$, Figure 8d. This general pattern was also evident in the 1m and 3m measurements and shows that the surf zone itself is a source of significant positive buoyancy flux.

Figure 8. Buoyancy Flux versus Various Parameters

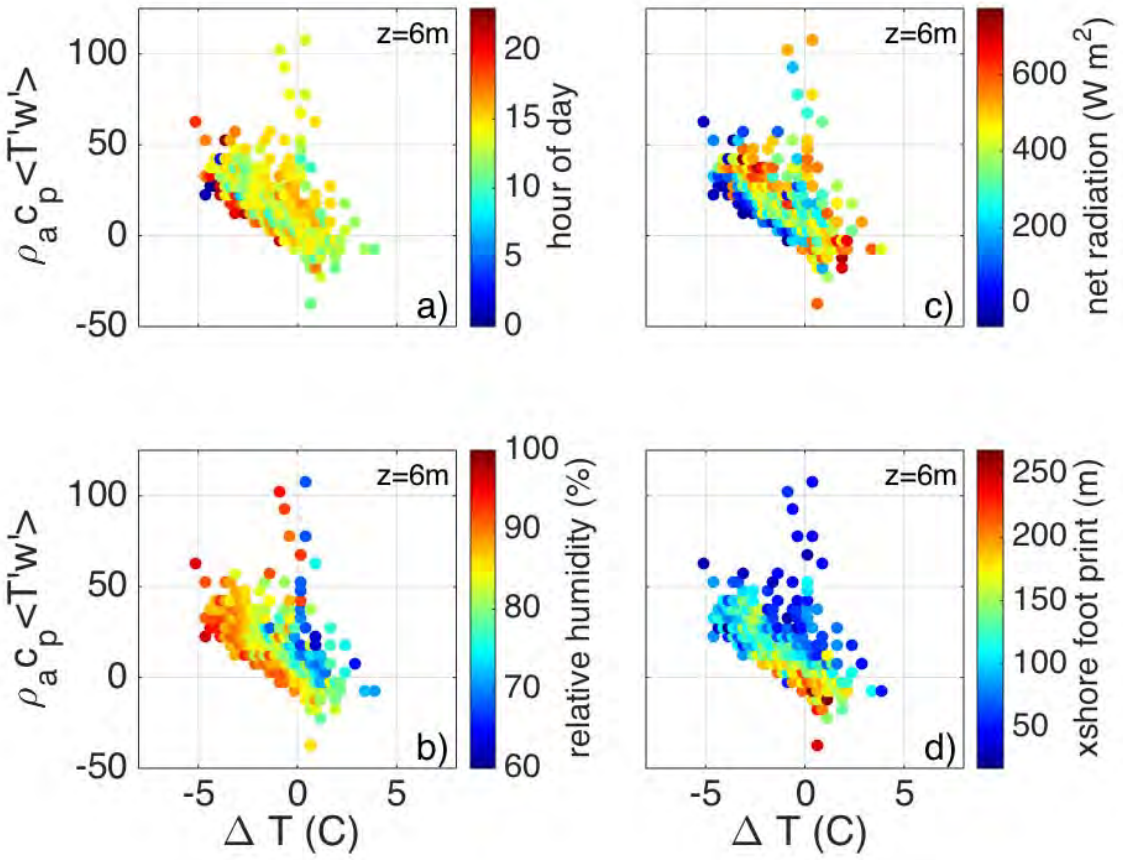

Buoyancy flux for the 6m sonic anemometer during deployment 4. The y-axis is buoyancy flux calculated according to equation (17). The x-axis is the temperature difference between the measurement height and the ocean surface temperature measured from the off shore array ($T_a - T_w$). Negative values indicate the ocean is warmer than the atmosphere and positive indicates that ocean temperatures are colder than the atmosphere. Data are shaded according to (a) hour of the day in local standard time (b) relative humidity at 6m (c) net radiation measured by the CNR-4 radiometer and (d) the cross shore distance from the tower towards the ocean that corresponds with the foot print calculation $x_{\max}$ from equation (18). The data has been filtered to include only onshore winds where the footprint, defined by equation (18), is over the water.

D. STRESS AND DRAG

As expected, the total wind stress, τ, increases with the wind speed, Figure 9a. The measured mean values range from 1.7 to 2.9 times larger than the predicted values based on Large and Pond (1981) or Smith (1988) bulk

formulas. This is consistent with Shabani et al. (2014) and Ortiz-Suslow et al. (2015). Both of these studies found that measured stresses were larger than expected from bulk formulas. For C_{DN}, results are mixed with the mean 1m C_{DN} slightly lower than Smith (1.08 versus 1.10) and the mean 6m C_{DN} slightly higher than Large and Pond (1.39 versus 1.36). The measured-3m drag was consistently higher than the either of the predicted values that were compared in this thesis with a mean of 1.52 (Figure 9)

Figure 9. Wind Stress and Drag Coefficients

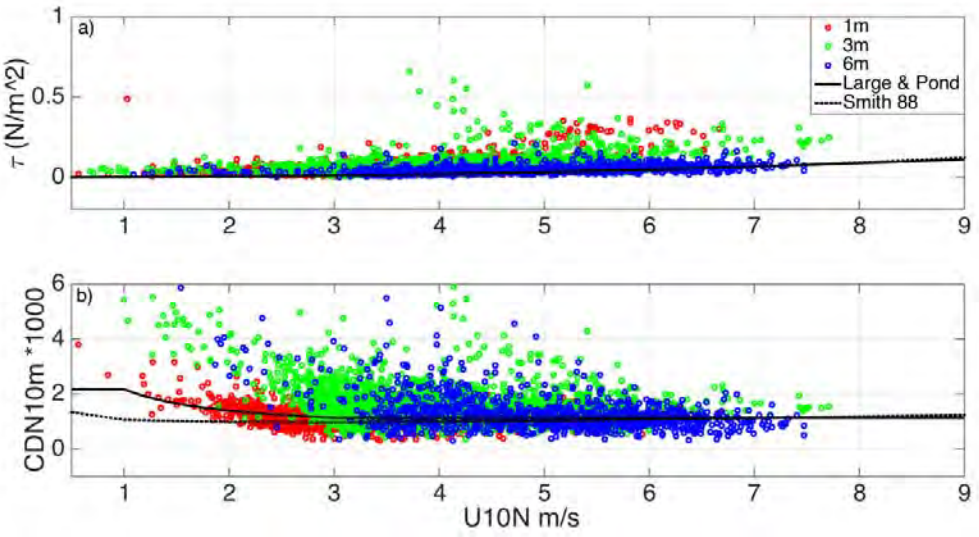

Wind stress τ (a) and 10m neutral drag (b) as a function of the 10m neutral wind speed. The solid black line represents expected open ocean values using Large and Pond (1981) as modified by Trebenth et al. (1990) to include winds <4ms. The dashed line represents the expected values using Smith (1988). Both τ and C_{DN} represent 15min averaged periods of the direct EC data and has been filtered to include only data from onshore winds between -80 to +10 degrees relative to shore normal.

Drag coefficients increase for low wind speeds in a similar fashion noted in previous studies (Geernaert el al. 1993; Zhu and Furst 2013; Ortiz-Suslow et al. 2015) and follow the general pattern of the Large and Pond curve (Figure 9b). However, the range is quite large almost zero to more than twice the expected

values of 1 to 1.5×10^3. This is in agreement with beach observations by Shabani et al. (2014)

E. STRESS DIRECTION

According to MOST, the stress and wind vectors should be aligned. However, it is now widely accepted that over the ocean the vector of τ varies widely, and is directed across or even opposite the mean wind flow (Grachev et al. 2001a). It is also accepted that the direction of the stress lies between the wind direction and swell direction (Geernaert et al. 1993; Rieder et al. 1996). Since open ocean winds and waves are generally aligned, the difference between the wind and swell vectors and the stress angle are relatively small and MOST remains valid. In the nearshore environment, however, stress angle can be as large as 90 degrees (Ortiz-Suslow et al. 2015).

For the current study, large deviations of $\pm 60^\circ$ occur for all sensor heights and across all four deployments (Figures 10a–d). This pattern is independent of wind speed signifying that the stress angle, α, is function of wind angle relative to the shore and swell. For shore normal winds, which are in general alignment with the swell direction, the stress angle tends to be positive and directed to the left of the wind. This is consistent with Grachev and Fairall (2001b), who also found that the stress angle tended to be directed to the left of the wind vector.

Figure 10. Relative Stress Direction (α)

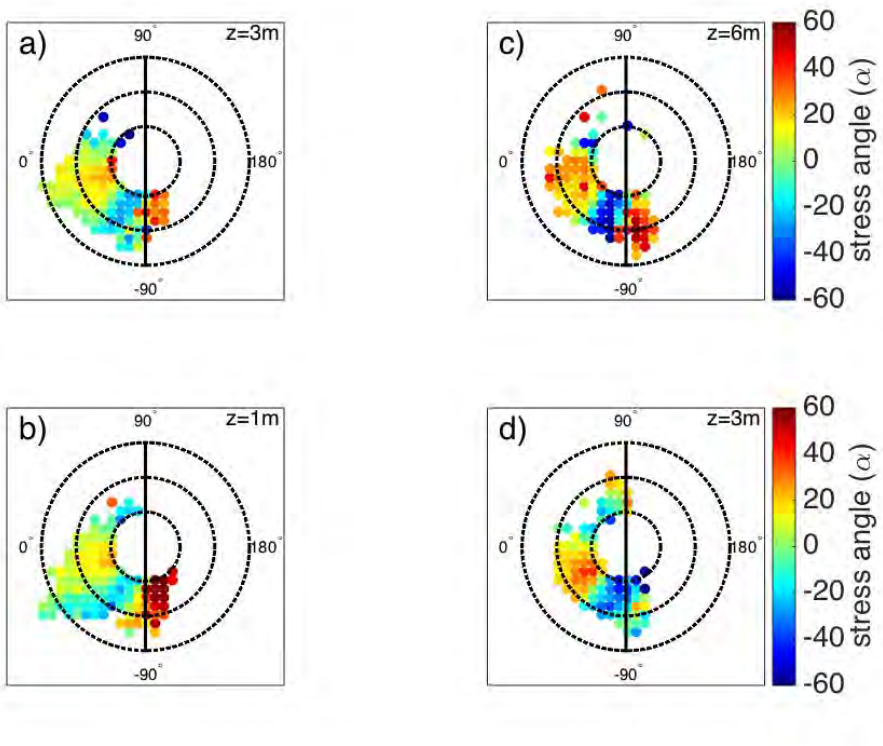

The magnitude and direction of the wind as measured by sonic anemometers deployed at (a) 3m during deployments 1–3, (b) corresponding 1m measurements for deployments 1–3, (c) and (d) the 6m and 3m measurements taken during deployment 4. The dashed range rings indicate wind speed in increments of 3m/s (3,6,9m/s). Directional headings are in the local coordinate system where 0 degrees is shore normal from the water. The solid vertical line from -90 and 90 is alongshore. The color shading represents α in degrees with positive (negative) values of indicating that the wind stress is directed to the left (right) of the mean wind vector.

For on shore winds, the stress, τ, does not exhibit any directional attributes; it is a function of wind speed, Figure 11. Offshore winds and along shore winds, most notably for the 6m sensor height, Figure 11c, have higher stress values than on shore winds due the roughness of the beach and surrounding landscape.

Figure 11. Stress (τ)

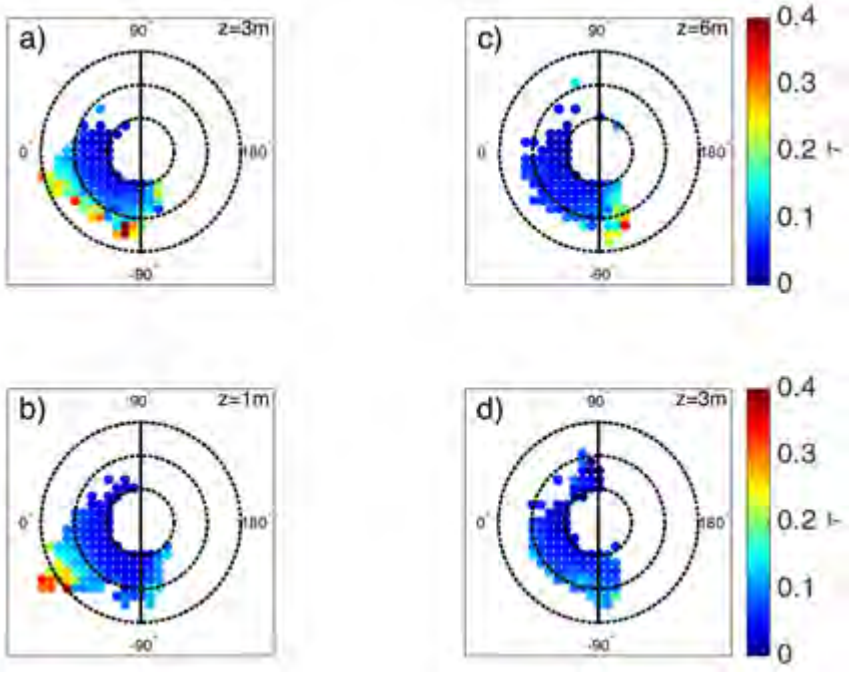

The magnitude and direction of the wind as measured by sonic anemometers deployed at (a) 3m during deployments 1–3, (b) corresponding 1m measurements for deployments 1–3, (c) and (d) the 6m and 3m measurements taken during deployment 4. The dashed range rings indicate wind speed in increments of 3m/s (3,6,9m/s). Directional headings are in the local coordinate system where 0 degrees is shore normal from the water. The solid vertical line from -90 and 90 is alongshore. The color shading represents τ.

For onshore winds, stability (z/L) also increases along with the wind speed, Figure 12. Near neutral stability is observed with the maximum winds Figures 12a and 12b. Along shore winds, which are traveling over the exposed beaches encounter the lowest stability values, Figure 12d.

Figure 12. Stability (z/L)

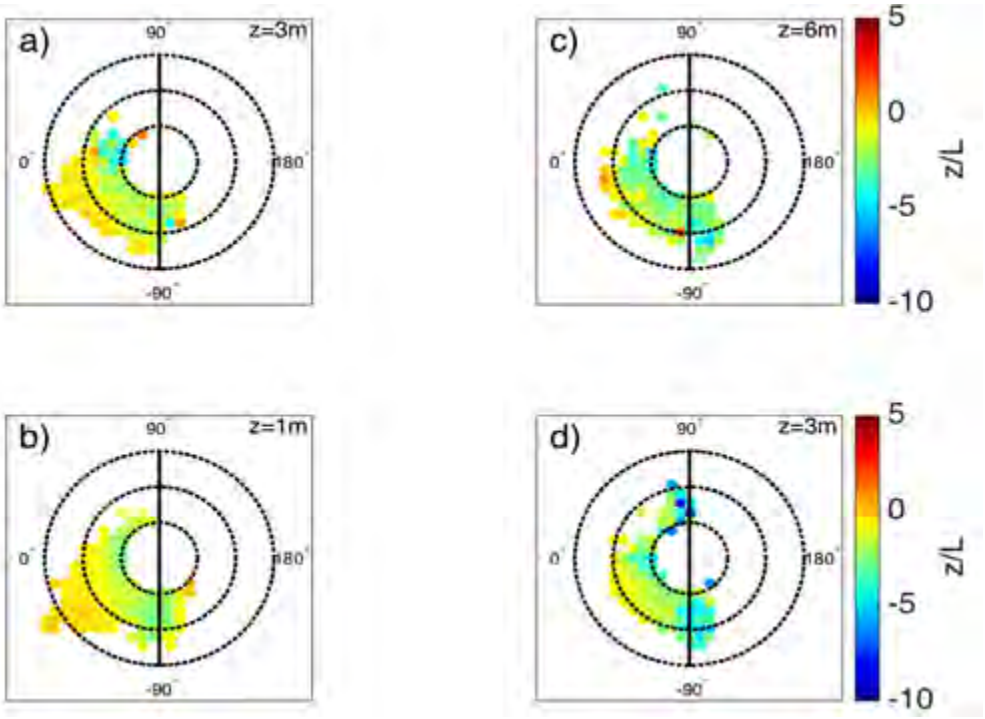

The magnitude and direction of the wind as measured by sonic anemometers deployed at (a) 3m during deployments 1–3, (b) corresponding 1m measurements for deployments 1–3, (c) and (d) the 6m and 3m measurements taken during deployment 4. The dashed range rings indicate wind speed in increments of 3m/s (3,6,9m/s). Directional headings are in the local coordinate system where 0 degrees is shore normal from the water. The solid vertical line from -90 and 90 is alongshore. The color shading represents stability parameter (z/L) with positive values indicating stable conditions and negative values indicating unstable conditions.

At times, the footprint of the flux measurements was predominately over the sandy beach and swash zone. Additionally, wave conditions varied over time as winter storm swells dissipated and gave way to more moderate swells associated with summer time high pressure in the eastern pacific. To test the impact these could have had on the stress angle, α for the 3m and 6m deployment heights, was bin averaged by both relative wind direction and significant wave height. Additionally, the data was filtered to include only data with a footprint ratio greater than one indicating the readings were predominately over the water.

The stress angle showed no significant overall dependence on offshore height Figures 13 a and 13b. The bin averaged magnitude of α, with over the water footprints, was consistent with the initial findings, Figures 10a, 10c, and 10d. Differences between α calculated for the 6m, Figure 13a, and 3m, Figure 13b, deployment heights were generally minimal and within 10° for all but the alongshore winds where the stress angle was 20° greater for 6m. It is believed that the similarity exists because of the wave heights are relatively similar owing to depth-limited wave breaking. Larger wave heights will result in a wider surf zone, but again this does not appear to have a statistically significant influence.

Figure 13. Stress Angle (α) Sensitivity to Wave Height

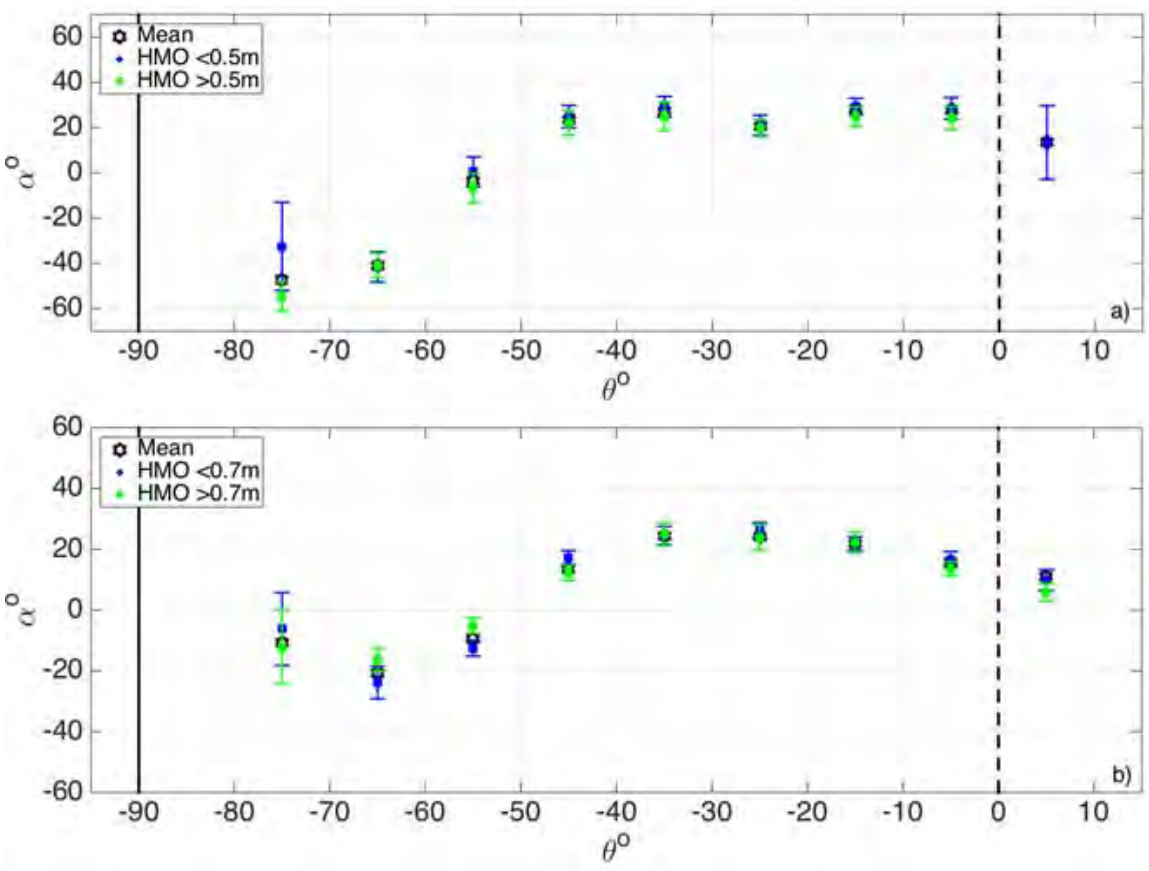

Relative stress angle α as a function of wind direction (θ) relative to the swell angle and shoreline in the local coordinate system for (a) 6m anemometer height during deployment 4 and (b) the 3m anemometer height during all 4 deployments. Plotted for each height is the mean value in each bin and the mean values corresponding with the lower and upper halves of the significant wave height distribution as measured just off shore. Note that the mean significant wave height for each plot is different owing to different deployment times. Wind direction is in the meteorological "from" convention, where wind from 0°, dashed vertical line, is directly on shore and winds from -90°, solid vertical line, are along shore from left to right. Data are binned 10° increments of θ and have been filtered to show only onshore winds $-80 < \theta < 10$ and where the flux footprint is over the water. Error bars represent the 95% confidence interval for each group of binned data.

As $|\theta|$ increases, not only does the magnitude of α change but also an inflection point exists around $|\theta| = 45^{\circ}$ where the sign of the stress switches. Potter (2015) found similar an inflection point noting that there was up to a 26% reduction in C_{DN} when the angle between wind and swell exceeded 45°.

Likewise, Shabani et al. (2014) found significant reduction in C_{DN} with along shore winds for $|\theta| = 45^{\circ}$ relative to the shoreline. Here, the minimum values for C_{DN} were associated with onshore winds, Figure 14. There is a reduction in C_{DN} from its maximum to the along shore value, the drop is not as significant as was expected, and in most cases it does not represent the minimum.

Figure 14. Neutral Drag (C_{DN}) versus Wind Direction (θ)

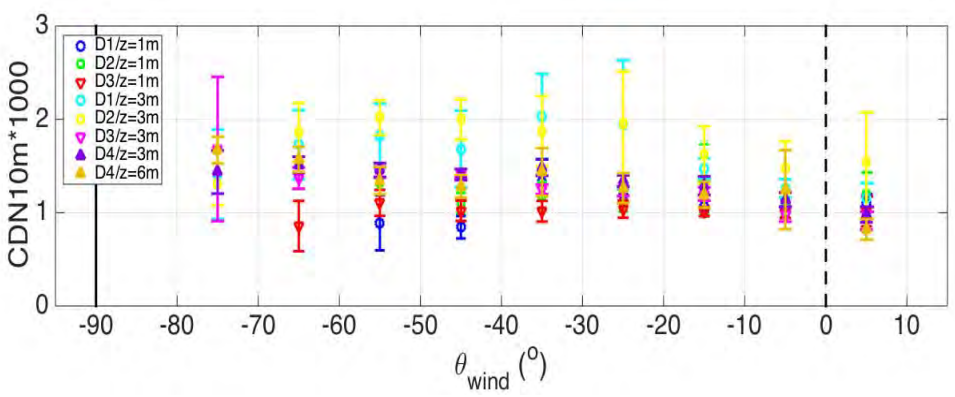

Mean 10m neutral drag (10^3) as a function of wind direction (θ) relative to the swell angle and shoreline in the local coordinate system for each of the eight individual anemometer elevation deployments. Wind direction is in the meteorological "from" convention, where wind from 0°, dashed vertical line, is directly on shore and winds from -90°, solid vertical line, are along shore from left to right. Data are binned 10° increments of θ and have been filtered to show only onshore winds $-80 < \theta < 10$ where the foot print indicates the measurement is for over the water. Error bars represent the 95% confidence interval for each bin.

The differences in alongshore drag is believed to be dependent upon the manner in which u_* was calculated. Bulk calculations of wind stress are estimated according to MOST, which states that the stress vector is aligned with the mean wind direction. By definition, therefore, the cross-stream component of the wind is assumed zero or negligible. Thus, reducing equations (3) and (4) to

$$\tau = -\rho_a \overline{u'w'} \tag{21}$$

$$u_* = \left(\overline{u'w'}^2\right)^{\frac{1}{4}}, \tag{22}$$

effectively reducing the magnitude of the stress, the stability functions, and ultimately the drag coefficient C_{DN}. Vickers et al. (2013) noted that many studies, even using direct measurements, do not provide specific details on their use of stream wise versus total stress components in the calculation of C_{DN}. To explore this, drag coefficients were calculated using both total and stream wise u_* following Vickers et al. (2013).

As expected, C_{DN} calculated using the total u_* was higher than stream wise u_*, Figure 15. It was also expected that the maximum sensitivity would correspond to the maximum values for α. Surprisingly, the opposite was true. For all deployments, the maximum difference between the two methods, from 0.25 to 0.65, occurred in the bin centered on $\theta = -45^\circ$. This is where α is a minimum, Figure 13. Additionally, when the winds are shore normal, and α is between 10°–20° to the left of the wind vector, there is no significant difference between the two drag calculations.

Figure 15. Drag Sensitivity to Total versus Streamwise Stress

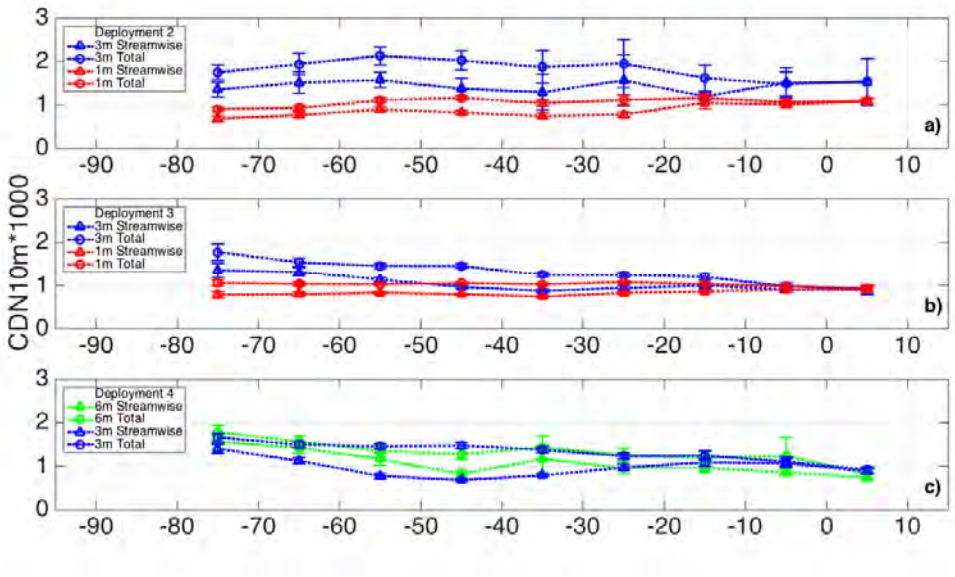

Calculations of the mean 10m neutral drag (10^3) as a function of wind direction (θ) relative to the swell angle and shoreline in the local coordinate system for the upper and lower anemometers for deployments 2 (a) 3 (b) and 4 (c). Circles represent drag calculated using the total u_* as defined in equation (5) and triangles represent drag calculated using the stream wise u_* as in equation (21). Wind direction is in the meteorological "from" convention, where wind from 0°, is directly on shore and winds from -90° are along shore from left to right. Data are binned in 10° increments of θ and have been filtered to show only onshore winds $-80 < \theta < 10$. Error bars represent the 95% confidence interval for each bin.

Wave height H_w also influences stress and drag calculations in bulk formulas and is used to parameterize the surface roughness and drag calculations over the open ocean (Taylor and Yelland 2001) as part of wave steepness. Wave steepness is defined as H_w / λ , where λ is the wavelength. As waves grow and accelerate, the wavelengths become longer and the steepness and drag decrease. Conversely, as waves approach the shore and decelerate, λ becomes shorter and the steepness and drag increase. Shabani et al. (2014) theorize that an apparent decrease in wave steepness could explain the decrease in C_{DN} with along shore winds. This apparent wave steepness is caused by a stream wise increase the distance between wave crests when the wind travels at an oblique angle to the waves.

To test the sensitivity of the measured drag to wave height C_{DN} was bin averaged by both relative wind direction and significant wave height. Additionally, observations were filtered to include only conditions when the footprint ratio greater than one (indicating the readings were predominately over the water). For the 6m sensor, C_{DN} increased as the wind angle increased, Figure 16a. Also, there was some sensitivity to the wave height; however, it was not statistically significant at the 95% confidence level. This is likely due the low range of significant wave heights observed, less than 1m. The 3m sensor, which covers nearly the entire study period, does show a noticeable decrease in C_{DN} as winds become more alongshore, Figure 16b. However, the alongshore values are 40% higher than the on shore values, and apparent wave steepness does not seem to be factor. For 66% of the direction bins, there is a statistically significant difference in C_{DN} between higher and lower wave heights for the 3m sensor, Figure 16b.

Figure 16. Drag Sensitivity to Wave Height

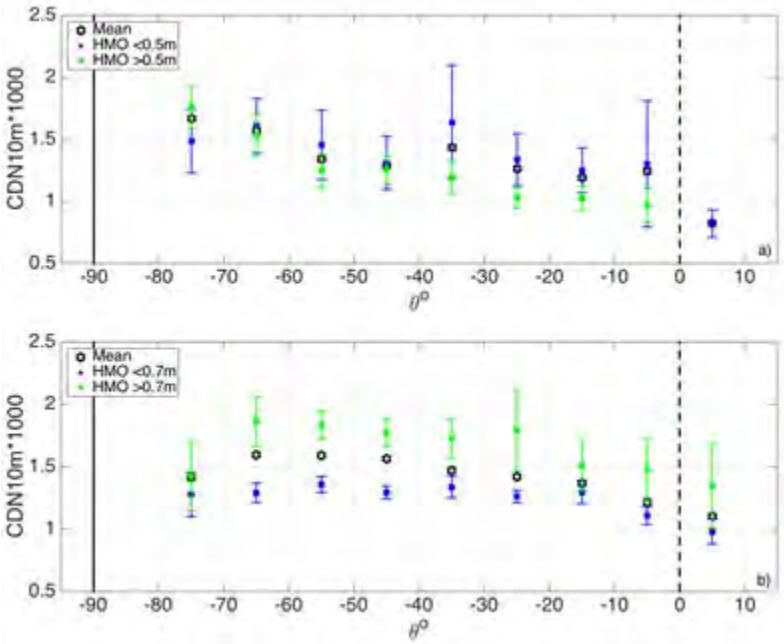

C_{DN} as a function of wind direction (θ) relative to the swell angle and shoreline in the local coordinate system for (a) 6m anemometer height during deployment 4 and (b) the 3m anemometer height during all 4 deployments. Plotted for each height is the mean value in each bin and the mean values corresponding with the lower and upper halves of the significant wave height distribution as measured just off shore. Note that the actual wave height breakpoint for each plot is different owing to different deployment time frames. Wind direction is in the meteorological "from" convention, where wind from 0°, dashed vertical line, is shore normal, on shore flow and winds from -90°, solid vertical line, are along shore from left to right. Data are binned 10° increments of θ and have been filtered to show only onshore winds $-80 < \theta < 10$ where the flux footprint is over the water. Error bars represent the 95% confidence interval for each group of binned data.

THIS PAGE INTENTIONALLY LEFT BLANK

V. CONCLUSIONS

An extensive study was performed on a sandy dissipative beach to explore the complex interactions of the solar cycle, nearshore waves/surf and air-ocean temperature differences. An eddy covariance Surf Flux Tripod was developed and deployed in the intertidal zone for this purpose, and resulted in the collection of 1088 hours of quality controlled flux data over the five-month duration.

The wind stress angle α was found to be highly dependent on the wind/swell crossing angle θ and independent of the stress magnitude, stability or significant wave height. It was shown that, in general, α was positive for $0^\circ > \theta > -45^\circ$ and the wind stress was directed to the left of the wind vector and that α was negative for $-45^\circ > \theta > -80^\circ$ and wind stress was directed to the right of the wind vector.

There was a marked decrease in the alongshore stress was not observed. Believing that this could be due to differences in the method used to calculate the friction velocity u_*, a sensitivity analysis was performed. The neutral drag coefficient C_{DN} was calculated using both total u_* as in equation (5) and stream wise only u_*, as in equation (22). It was found unexpectedly that when winds and waves are in general alignment, as would be typical over the open ocean, there was no significant difference between the two different drag coefficients. The maximum difference was seen when the wind angle, relative to the swell direction was 45°,where the stress and wind vectors are most closely aligned.

An analysis of the stability of the nearshore environment was also undertaken. The nearshore environment was found to be almost always unstable, with greater than 88% of all measurements being considered convectively unstable. This is a stark difference to what has been seen in the open ocean where conditions are almost always near neutral. This was in part due to persistent nighttime air-sea temperature differences, which promoted

positive buoyancy flux readings well into the nighttime hours. Buoyancy flux was examined as a function of the cross-shore flux footprint distance, $x_{\max}$. Buoyancy flux decreased for all air-sea temperature difference ranges and all deployment heights as $x_{\max}$ increased. This indicates that the more turbid surf zone produces considerably more buoyancy flux than ocean does just off shore where the buoyancy flux values decrease significantly and become negative.

LIST OF REFERENCES

Aubinet, M., T. Vesala, and D. Papale, 2012: *Eddy covariance: A practical guide to measurement and data analysis*. Springer Science & Business Media, 451pp.

Bernardes, M., and N. L. Dias, 2009: The alignment of the mean wind and stress vectors in the unstable surface layer. *Boundary-Layer Meteorol.*, **134**, 41–59, doi:10.1007/s10546-009-9429-8.

Businger, J. A., J. C. Wyngaard, Y. Izumi, and E. F. Bradley, 1971: Flux-Profile Relationships in the atmospheric surface layer. *J. Atmos. Sci.*, **28**, 181–189, doi:10.1175/1520-0469(1971)028<0181:FPRITA>2.0.CO;2.

Charnock, H., 1955: Wind stress on a water surface. *Q. J. R. Meteorol. Soc.*, **81**, 639–640.

Edson, J. B., and Coauthors, 2013: On the exchange of momentum over the open ocean. *J. Phys. Oceanogr.*, **43**, 1589–1610, doi:10.1175/JPO-D-12-0173.1.

Fairall, C. W., E. F. Bradley, J. E. Hare, A. A. Grachev, and J. B. Edson, 2003: Bulk parameterization of air–sea fluxes: updates and verification for the COARE Algorithm. *J. Clim.*, **16**, 571–591, doi:10.1175/1520-0442(2003)016<0571:BPOASF>2.0.CO;2.

Gash, J. H. C., 1986: A note on estimating the effect of a limited fetch on micrometeorological evaporation measurements. *Boundary-Layer Meteorol.*, **35**, 409–413, doi:10.1007/BF00118567.

Geernaert, G. L., S. E. Larsen, and F. Hansen, 1987: Measurements of the wind stress, heat flux, and turbulence intensity during storm conditions over the North Sea. *J. Geophys. Res.*, **92**, 13127, doi:10.1029/JC092iC12p13127.

——, K. L. Davidson, S. E. Larsen, and T. Mikkelsen, 1988: Wind stress measurements during the Tower Ocean Wave and Radar Dependence Experiment. *J. Geophys. Res.*, **93**, 13913, doi:10.1029/JC093iC11p13913.

——, F. Hansen, M. Courtney, and T. Herbers, 1993: Directional attributes of the ocean surface wind stress vector. *J. Geophys. Res.*, **98**, 16571, doi:10.1029/93JC01439.

Grachev, A., C. Fairall, J. Hare, J. Edson, and S. Miller, 2003: Wind stress vector over ocean waves. *J. Phys. Oceanogr.*, **33**, 2408–2429, doi:10.1175/1520-0485(2003)0332.0.CO;2.

——, ——, J. E. Hare, J. B. Edson, W. Hole, and W. Hole, 2001a: Wind stress vector over sea waves. Reprints, *11th Conf. on Interaction of the Sea and Atmosphere*, San Diego, CA, Amer. Meteor. Soc., 1.4

——, ——, 2001b: Upward momentum transfer in the marine boundary layer. *J. Phys. Oceanogr.*, **31**, 1698–1711, doi:10.1175/1520-0485(2001)031<1698:UMTITM>2.0.CO;2.

Hendrickson, J., and J. MacMahan, 2009: Diurnal sea breeze effects on inner-shelf cross-shore exchange. *Cont. Shelf Res.*, **29**, 2195–2206, doi:10.1016/j.csr.2009.08.011.

Johnson, D.,1977: The late quaternary climate of coastal California: Evidence for an ice age refugium. *Quaternary Res.* **8**,154–179

Kader, B. A., and A. M. Yaglom, 2006: Mean fields and fluctuation moments in unstably stratified turbulent boundary layers. *J. Fluid Mech.*, **212**, 637, doi:10.1017/S0022112090002129.

Kaimal, J. C., and J. E. Gaynor, 1991: Another look at sonic thermometry. *Boundary-Layer Meteorol.*, **56**, 401–410, doi:10.1007/BF00119215.

Kara, A. B., H. E. Hurlburt, and A. J. Wallcraft, 2005: Stability-dependent exchange coefficients for air–sea fluxes*. *J. Atmos. Ocean. Technol.*, **22**, 1080–1094, doi:10.1175/JTECH1747.1.

——, J. C. Wyngaard, Y. Izumi, and O. R. Cote, 1972: Spectral characteristics of surface-layer turbulence. *Q. J. R. Meteorol. Soc.*, **98**, 563–589.

Large, W., and S. Pond, 1981: Open ocean momentum flux measurements in moderate to strong winds. *J. Phys. Oceanogr.*, **11**, 324–336, doi:10.1175/1520-0485(1981)0112.0.CO;2.

Liu, W. T., X. Xie, and P. P. Niiler, 2007: Ocean–Atmosphere Interaction over Agulhas Extension Meanders. *J. Clim.*, **20**, 5784–5797, doi:10.1175/2007JCLI1732.1.

Lo, A. K., and G. A. McBean, 1978: On the relative errors in methods of flux calculations. *J. Appl. Meteorol.*, **17**, 1704–1711, doi:10.1175/1520-0450(1978)017<1704:OTREIM>2.0.CO;2.

MacMahan, J. H., E. B. Thornton, T. P. Stanton, and A. J. H. M. Reniers, 2005: RIPEX: Observations of a rip current system. *Mar. Geol.*, **218**, 113–134, doi:10.1016/j.margeo.2005.03.019.

Monin, A. S., and A. M. Obukhov, 1954: Basic laws of turbulent mixing in the surface layer of the atmosphere. *Contrib. Geophys. Inst. Slovak Acad. Sci.*, **24**, 163–187.

National Oceanic and Atmospheric Administration, 2011: Datums for 9413450, Monterey CA. Accessed 01 January 2015. [Available online at http://tidesandcurrents.noaa.gov/datums.html?id=9413450]

Ortiz-Suslow, D. G., B. K. Haus, N. J. Williams, N. J. M. Laxague, A. J. H. M. Reniers, and H. C. Graber, 2015: The spatial-temporal variability of air-sea momentum fluxes observed at a tidal inlet. *J. Geophys. Res. Ocean.*, **120**, 660–676, doi:10.1002/2014JC010412.

Paulson, C. A., 1970: The mathematical representation of wind speed and temperature profiles in the unstable atmospheric surface layer. *J. Appl. Meteorol.*, **9**, 857–861.

Paw, U., D. Baldocchi, T. Meyers, and K. Wilson, 2000: Correction of eddy-covariance measurements incorporating both advective effects and density fluxes. *Bound. Layer Meteorol.*, **97**, 487–511.

Potter, H., 2015: Swell and the drag coefficient. *Ocean Dyn.*, **65**, 375–384, doi:10.1007/s10236-015-0811-4.

Reichl, B. G., T. Hara, and I. Ginis, 2014: Sea state dependence of the wind stress over the ocean under hurricane winds. *J. Geophys. Res. Ocean.*, **119**, 30–51, doi:10.1002/2013JC009289.

Rieder, K. F., and J. A. Smith, 1998: Removing wave effects from the wind stress vector. *J. Geophys. Res.*, **103**, 1363, doi:10.1029/97JC02571.

——, ——, and R. A. Weller, 1994: Observed directional characteristics of the wind, wind stress, and surface waves on the open ocean. *J. Geophys. Res.*, **99**, 22589, doi:10.1029/94JC02215.

Rufencach, C. L., J. J. Bates, and S. Tosini, 1998: ERS-1 scatterometer measurements. I. The relationship between radar cross section and buoy wind in two oceanic regions. *IEEE Trans. Geosci. Remote Sens.*, **36**, 603–622, doi:10.1109/36.662742.

Schmid, H. P., 1994: Source areas for scalars and scalar fluxes. *Boundary-Layer Meteorol.*, **67**, 293–318, doi:10.1007/BF00713146. http://dx.doi.org/10.1007/BF00713146.

Schuepp, P. H., M. Y. Leclerc, J. I. MacPherson, and R. L. Desjardins, 1990: Footprint prediction of scalar fluxes from analytical solutions of the diffusion equation. *Boundary-Layer Meteorol.*, **50**, 353–373.

Shabani, B., P. Nielsen, and T. Baldock, 2014: Direct measurements of wind stress over the surf zone. *J. Geophys. Res. Ocean.*, **119**, 2949–2973, doi:10.1002/2013JC009585.

Smith, S. D., 1980: Wind stress and heat flux over the ocean in gale force winds. *J. Phys. Oceanogr.*, **10**, 709–726, doi:10.1175/1520-0485(1980)010<0709:WSAHFO>2.0.CO;2.

——, 1988: Coefficients for sea surface wind stress, heat flux, and wind profiles as a function of wind speed and temperature. *J. Geophys. Res.*, **93**, 15467, doi:10.1029/JC093iC12p15467.

——, and Coauthors, 1992: Sea surface wind stress and drag coefficients: The hexos results. *Boundary-Layer Meteorol.*, **60**, 109–142, doi:10.1007/BF00122064. http://dx.doi.org/10.1007/BF00122064.

Smithsonian Institution., S., C. Abbe, C. F. Marvin, A. McAdie, and A. Guyot, 1897: *Smithsonian meteorological tables: Based on Guyot's meteorological and physical tables*. Smithsonian Institution, Washington, DC

Thornton, E. B., J. J. Galvin, F. L. Bub, and D. P. Richardson, 1976: Kinematics of breaking waves. *Coast. Eng. Proc.*, **1**, doi:10.9753/icce.v15.%p.

Trenberth, K., W. Large, and J. Olson, 1990: The mean annual cycle in global ocean wind stress. *J. Phys. Oceanogr.*, **20**, 1742–1760, doi:10.1175/1520-0485(1990)0202.0.CO;2.

Vickers, D., L. Mahrt, and E. L. Andreas, 2013: Estimates of the 10-m neutral sea surface drag coefficient from aircraft eddy-covariance measurements. *J. Phys. Oceanogr.*, **43**, 301–310, doi:10.1175/JPO-D-12-0101.1.

Wilczak, J., S. Oncley, and S. Stage, 2001: Sonic Anemometer Tilt Correction Algorithms. *Boundary-Layer Meteorol.*, **99**, 127–150, doi:10.1023/A:1018966204465.

Yelland, M., and P. K. Taylor, 1996: Wind stress measurements from the open ocean. *J. Phys. Oceanogr.*, **26**, 541–558.

Zemba, J., and C. A. Friehe, 1987: The marine atmospheric boundary layer jet in the Coastal Ocean Dynamics Experiment. *J. Geophys. Res.*, **92**, 1489, doi:10.1029/JC092iC02p01489.

Zhang, F. W., W. M. Drennan, B. K. Haus, and H. C. Graber, 2009: On wind-wave-current interactions during the Shoaling Waves Experiment. *J. Geophys. Res.*, **114**, C01018, doi:10.1029/2008JC004998.

Zhu, P., and J. Furst, 2013: On the parameterization of surface momentum transport via drag coefficient in low-wind conditions. *Geophys. Res. Lett.*, **40**, 2824–2828, doi:10.1002/grl.50518.

INITIAL DISTRIBUTION LIST

1. Defense Technical Information Center
   Ft. Belvoir, Virginia

2. Dudley Knox Library
   Naval Postgraduate School
   Monterey, California